Journal of Engineering Physics and Thermophysics, Vol. 82, No. 3, 2009

CALCULATION OF UNSTEADY FLOW PAST A CUBE ON THE WALL OF A NARROW CHANNEL USING URANS AND THE SPALART–ALLMARAS TURBULENCE MODEL

S. A. Isaev and D. A. Lysenko

UDC 532.517.4

The results of numerical simulation of fully developed turbulent flow in a channel with the cube on the lower wall (for the characteristic Reynolds number Re = 40,000) within the framework of the traditional approach to the solution of unsteady Reynolds-averaged Navier–Stokes equations (URANS) in combination with the semiempirical Spalart–Allmaras turbulence model (with a correction for rotation) have been presented. A detailed comparative analysis of the results of numerical simulation of local and integral flow characteristics and the Martinuzzi experimental data has shown that the self-oscillating regime of flow past the cube is a superposition of oscillations of the arms of a horseshoe vortex and the rear arched and detached vortex structures. Using fast Fourier transformation, it has been found that the oscillations are of a bimodal character in the longitudinal and vertical directions, whereas in the transverse direction, they are of a unimodal character.

Keywords: *separated flow, turbulence, cube in a channel, self-oscillating regime, experiment, calculation, URANS, Spalart–Allmaras model.*

Introduction. The problem on unsteady flow past a cube in a narrow channel with the fully developed turbulent flow being formed at the inlet is of particular interest for testing today's calculation algorithms of computational hydrodynamics. In this case channel flow is of a self-oscillating character and is distinguished by a complex vortex structure (Fig. 1). Flow separation begins ahead of the cube and further develops from its frontal face side and on the lateral walls. A horseshoe vortex that interacts with the near wake of the cube results. We recognize the following basic large-scale flow elements for their subsequent analysis and comparison to experimental data: 1) a horseshoe vortex; 2) a vortex ensemble consisting of a vortex attached to the face side of the cube and two columnar vortices near the lateral walls; 3) a rear detached vortex; 4) an attached vortex behind the end wall of the cube, which is not identified in the Martinuzzi experiment, as should be noted, but is visualized in many calculations; 5) an arched vortex with two oppositely rotating bends, which is formed in the near wake.

Experimental data to which we compare results of numerical investigations were obtained by Martinuzzi [1] and have been introduced into the ERCOFTAC (European Research Community on Flow, Turbulence and Combustion) databank [2]. About ten large-scale numerical investigations based on solution of steady and unsteady Reynolds-averaged Navier–Stokes equations (RANS/URANS) and on application of the large-eddy model (see, e.g., [3–5]) have been carried out over a period of 15 years. It is noteworthy that, except for the results obtained by Durbin with the V2F turbulence model [6], none of the works gives satisfactory agreement between the results of calculations within the framework of the RANS/URANS methodology and the experimental data.

This work is primarily aimed at substantiating the applicability of the URANS approach to the prediction of turbulent separated flows. The commercial FLUENT v6.3 package [7] is used. Preliminary verification and approval of the package with a catalog of semiempirical models realized in it, which were carried out on two-dimensional test problems such as flow past a circular cylinder [8] and circulation flow in a square cavity with a moving upper boundary [9, 10], have shown satisfactory correlation with experimental data, when the two-parametric model of shear-stress transfer MSST and the Spalart–Allmaras (SA) vortex-viscosity model were selected. It has been shown in [8–10] that the SA model in its traditional formulation substantially overstates turbulent-viscosity values, which renders it unsuitable for calculations of turbulent separated flows. For further testing, we have selected the SA model modified with allowance for rotation.

St. Petersburg State University of Civil Aviation, 38 Piloty Str., St. Petersburg, 196210, Russia; email: isaev3612@yandex.ru. Translated from Inzhenerno-Fizicheskii Zhurnal, Vol. 82, No. 3, pp. 492–499, May–June, 2009. Original article submitted May 10, 2007; revision submitted October 19, 2008.

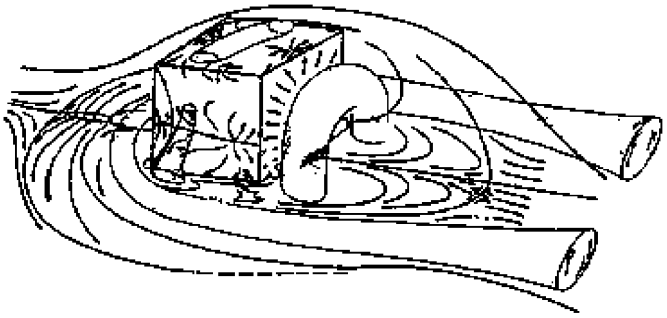

Fig. 1. Diagram of the basic large-scale flow elements occurring in the case of flow past a cube.

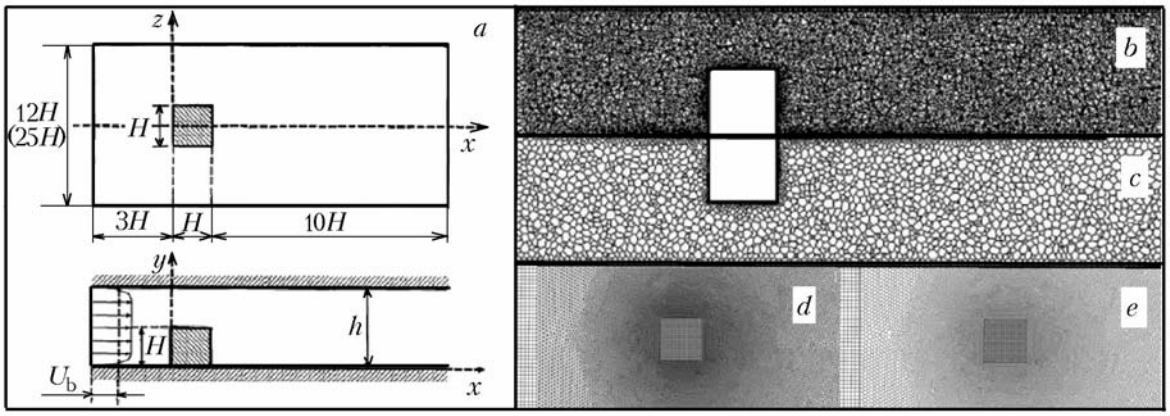

Fig. 2. Diagram of the computational domain (a), unstructured tetrahedral (b and d), and polyhedral (c and e) finite-element grids in the central longitudinal section (b and c) and on the lower channel wall (d and c).

Objective of the Work. (1) Investigate fully developed turbulent flow with a cube mounted into the lower wall (for Reynolds number calculated from the edge of the cube H and the mean-mass velocity U_b Re = 40,000) using URANS and the modified one-parameter SA turbulence model, (2) classify large-scale flow elements and make a detailed comparison of the numerical results for local and integral flow characteristics and the Martinuzzi experimental data [1], and (3) analyze the suitability of the URANS methodology for calculation of three-dimensional periodic turbulent separated flows.

Formulation of the Problem. The computational domain is selected from the conditions of physical experiment [1]. The edge of the cube, equal to H = 0.025 m, is taken as the characteristic linear dimension. The channel height is $h = 2H$; the length of the computational domain is $L = 14H$ in the longitudinal direction and $W = 12H$ in the transverse direction; the cube is at a distance $3H$ from the inlet boundary (Fig. 2a). It is noteworthy that although in the Martinuzzi experiment, the channel width is $25H$, in numerous calculations (see, e.g., [3–5]) the channel is artificially contracted to 3–9 calibers without explaining the reasons for this act, which can be due to savings in computer time. In the present work, we additionally consider a computational domain with a transverse dimension equal to $W = 25H$ (Fig. 2a) for investigation of the influence of the channel width. We use three unstructured tetrahedral (Nos. 1–3) and one polyhedral (No. 4) computational grids whose basic characteristics are given in Table 1. The general view of the tetrahedral grid (No. 1) and the polyhedral grid based on it (No. 4) in the longitudinal midsection and on the lower wall (top view) of the channel is shown in Fig. 2b and c and Fig. 2d and e respectively. Near the channel and cube walls, each computational grid has a separated viscous-sublayer zone consisting of prismatic elements (with the following parameters: number of rows 10, dimension of the first grid 0.0008, and growth factor 1.5), which ensures an average value of the parameter of $y^+ \sim 0.6$. The number of nodes varies from 0.9 to 3.1 mln, whereas the number of the elements varies from 1.2 to 4.2 mln (see Table 1).

TABLE 1. Description of the Employed Computational Grids

Grid number	Dimension of the channel ($L \times W \times h$)	Grid type	Number of nodes	Number of elements	y^+			Time step
					min	max	average	
1	$14 \times 12 \times 2$	Tetra	984 897	2 422 131	0.10	1.47	0.69	0.0767
2	$14 \times 12 \times 2$	Tetra	1 707 795	4 227 229	0.09	1.95	0.60	0.0575
3	$14 \times 25 \times 2$	Tetra	1 115 801	2 577 402	0.09	1.46	0.68	0.0767
4	$14 \times 25 \times 2$	Poly	3 133 121	1 272 940	0.10	1.62	0.69	0.0767

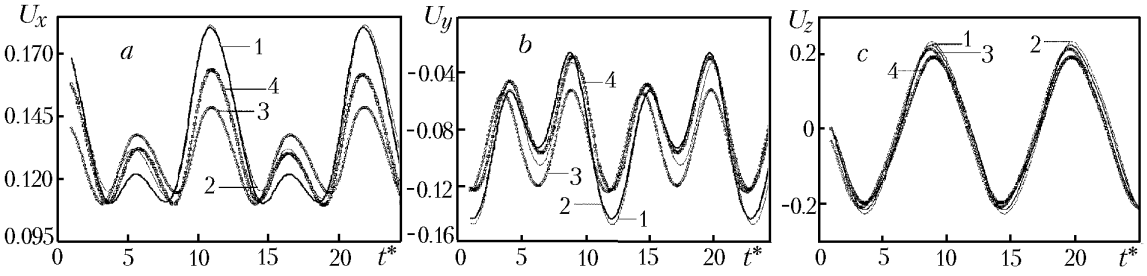

Fig. 3. Distributions of the local characteristics of flow: the horizontal (a), vertical (b), and lateral (c) velocity components as functions of the time depending on the employed computational grid Nos. 1–4 according to Table 1.

The mean-mass inlet velocity U_b of the incompressible-fluid flow is selected as the scale of making the parameters dimensionless analogously to [1] (Fig. 1a). The experimental velocity profile is prescribed at the inlet boundary. The intensity and characteristic scale of turbulence at the inlet are set equal to 1.5% and 0.025 m respectively. Soft boundary conditions are specified at the outlet boundary, symmetry conditions are set at the lateral boundaries, and sticking conditions are specified on the walls in flow.

Certain Aspects of Numerical Simulation. Using the finite-volume factorized method we solve a URANS system for an incompressible viscous fluid with an algebraic multigrid accelerator; the implementation of the method is based on the additive-correction strategy [7, 12]. To close the system of equations we use a low-Reynolds SA model [11] with a rotation correction. The term with a pressure gradient is discretized by a second-order approximation scheme, whereas the convective terms of the transfer equations are represented according to the Leonard quadratic upwind scheme (QUICK) [13]. The velocity and pressure fields are matched with a centered computational template within the framework of the Rhee–Chou approach [14]. Also, we use, in the algorithm, a SIMPLEC pressure-correction procedure [15] and an implicit iteration algorithm of the second order of approximation [16] for physical-time integration.

In the previous works carried out both using the large-eddy model [3, 4] and within the framework of the URANS methodology [5], a time step of 0.05 was used. In the present work, we have selected a time step of 0.0767 for computational grid Nos. 1, 3, and 4 and of 0.0575 for grid No. 2, which is acceptable since it ensures integration of one period of the self-oscillating regime in about 140 times steps.

It is common knowledge that the disagreement between experimental data and numerical results is determined by two groups of errors: 1) "model" errors due to the inadequate assumptions made in selecting one turbulence model or another and 2) "discretization" errors caused by the inadequate resolution of the employed finite-element grids and computational methods. Whereas the errors of the first group are assumed to be "systematic" under certain assumptions, e.g., for a fixed computational methodology, "discretization" errors are controlled by the method of adaptation (increase in the resolution) of a computational grid.

The grid independence of results of this numerical investigation is confirmed by: 1) the use of different grid structures (tetrahedral (Nos. 1–3) and polyhedral (No. 4) grids) and a virtually twofold increase in the number of nodes (or the resolution) of grid No. 1 — from 0.9 mln to 1.7 mln (grid No. 2) and 2) satisfactory agreement (with an error of ~10% in amplitude and of 3–5% in frequency) in the distribution of the local-velocity components (three velocity components (Fig. 3a, b, and c) obtained at a point with coordinates (3, 0.5, 0) are compared in this work.

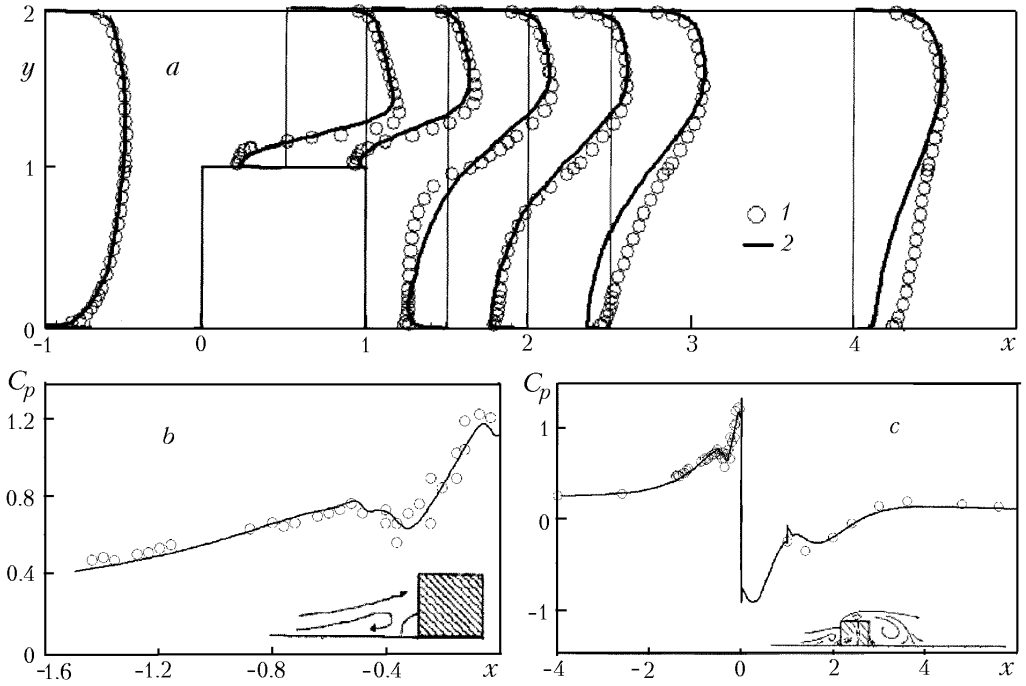

Fig. 4. Comparison of the profiles of the time-averaged longitudinal velocity component (a) in seven cross sections with longitudinal coordinates of −1.0, 0.5, 1.0, 1.5, 2.0, 2.5, and 4.0 and of the pressure coefficient near the cube (b) and throughout the computational domain (c) in the channel midsection (z = 0), which have been obtained experimentally (1) and numerically (2); b and c, diagrams of flow past the cube.

Analysis of Results. Some of the results obtained are presented in Figs. 4–6.

To compare the local flow characteristics we use the time-averaged local profiles of the horizontal velocity component (Fig. 4a) in seven selected vertical cross sections (having longitudinal coordinates of −1.0, 0.5, 1.0, 1.5, 2.0, 2.5, and 4.0) and the distribution of the pressure coefficient C_p on the lower channel wall (Fig. 4b and c) in the midsection of the computational domain (z = 0). A comparison of the experimental (1) and numerical (2) data for the longitudinal velocity component shows that in the first cross sections, the velocity components agree quite satisfactorily (the average error amounts to less than 5%), whereas in the last two cross sections, we observe certain mismatches. The disagreement amounts to ~10–15%, which is primarily due to the nearly 20% overstatement of the dimension of the rear detached vortex zone. The calculated and experimental distributions of the pressure coefficient (Fig. 4b and c) on the lower channel wall are in good agreement. A detailed analysis of the C_p distribution in front of the cube (Fig. 4b) shows that the position of the horseshoe vortex is determined within the framework of the computational methodology (URANS + SA) quite accurately (with an error of ~7.5%.)

The location of the forward saddle point S (X_f) corresponding to the position of the attached horseshoe vortex, the dimensions of the rear attached N (X_{r1}) and detached R (X_{r2}) vortices, and the Strouhal number are selected as the considered integral characteristics of the separated flow near the cube (Fig. 5). Generalized data are tabulated (Table 2); the same table also gives results obtained in computational investigations [3–5] and experimental data [1, 2]. Thus, in this numerical experiment, we are able to correctly identify the basic large-scale structural elements: the attached forward vortex (F) and separated recirculation zone behind the cube (R), the lateral (E) and attached upper (Top) vortices, and the arched vortex structure (B) (Fig. 5a and b). Additionally (Fig. 5d) we reveal, in the calculations, the rear attached vortex (N) which is absent in the experimental data on flow visualization [1] but is obtained in numerical investigations [3–5].

A comparison of the position of the detached vortices (attachment point C) behind the cube (Fig. 5b and c) and the data in Table 2 shows that the computational methodology used tends to overstate the dimension of the back

TABLE 2. Comparison of the Integral Flow Characteristics

Authors	Year	Method	X_f	X_{r1}	X_{r2}	St
Martinuzzi and Hussein [1, 2]	1993	Experiment	1.04	—	1.61	0.145
Rodi et al. [4]	1997	LES	1.00	0.13	1.43	—
Shah and Fersiger [5]	1997	LES	1.08	0.16	1.69	—
Iaccarino et. al. [3]	2003	URANS-V2F	0.73	0.20	1.88	0.170
This work	2008	URANS-SÀ	0.96	0.23	2.08	0.09; 0.175—0.185

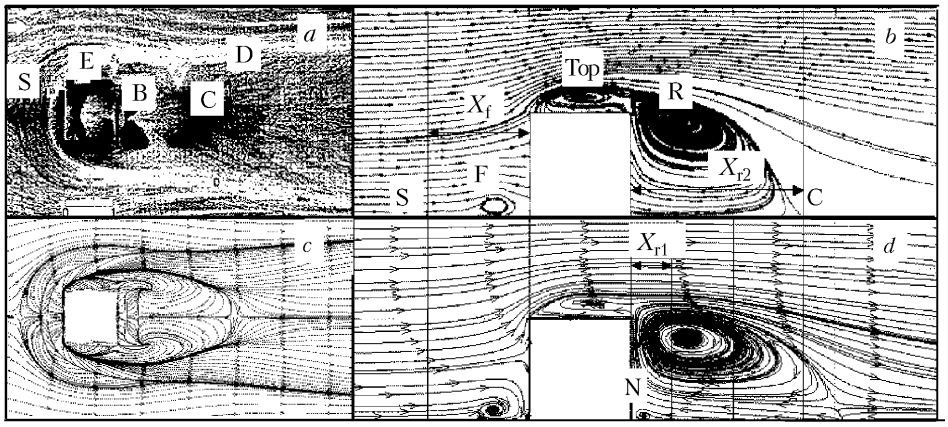

Fig. 5. Comparison of the time-averaged patterns of spreading of the fluid on the lower wall (a and c) and in the channel midsection (b and d): a and b) experiment; c and d) calculation.

separated zone (X_{r2}) by nearly 20% (Fig. 5c and d). It is noteworthy that analogous results are obtained with URANS and the V2F turbulence model [6] where the disagreement with the experimental data is of the order of 17%. The attached horseshoe vortex, as has already been noted, is predicted quite accurately. The position of the frontal saddle point S is predicted with an error of the order of 7%. In Fig. 5c, we can identify the arched vortex structure the wakes of whose two bends are at a distance of ~0.35 from the back wall of the cube, which quite accurately corresponds to experimental visualization (Fig. 5a). The position of the rear attached vortex N (X_{r1}) is in satisfactory agreement with the results obtained by Durbin [3].

We take the fast Fourier transform of three velocity components presented in Fig. 3a, b, and c to analyze the frequency characteristics of the self-oscillating process. For the transverse velocity component (U_z), the Strouhal number is St = 0.09. This velocity component has a pronounced unimodal distribution and, apparently, corresponds to transverse oscillations of the arms of the horseshoe vortex (Fig. 6). The longitudinal (U_x) and vertical (U_y) velocity components follow bimodal curves with dominant Strouhal numbers St = 0.09 and St = 0.175–0.185.

Let us analyze the self-oscillating motion of the arched and detached vortices on one period (St = 0.09) (Fig. 6). Two wakes of the left and right (relative to the flow direction) bends of the arched vortex are clearly seen on the instantaneous patterns of spreading (points b1 and b2 respectively). It is noticeable that the right bend of the vortex executes translational horizontal streamwise motion during the half-period (from $t^* = 1/8T$ to $t^* = 1/2T$), whereas the left bend remains on the spot. During the half-period that follows (from $t^* = 5/8T$ to $t^* = T$), the character of motion is reversed: the left bend of the vortex begins translational horizontal motion, whereas the wake of the right bend remains on the spot. Analogously we can analyze the motion of the large-scale detached vortex whose wake on the lower wall is denoted as the saddle point s. In the first 3/8 of a period, the saddle point executes oscillating motions, being to the left of the cube. Next, at the instant of time $t^* = 1/2T$, the saddle point shifts to the right where it executes oscillations during the following 3/8 of a period.

Thus, the calculated fluid flow in the channel with a cube on the lower wall is of a complex unsteady periodic character with two dominant Strouhal numbers St = 0.09 and St = 0.175–0.185. It is noteworthy that there is a

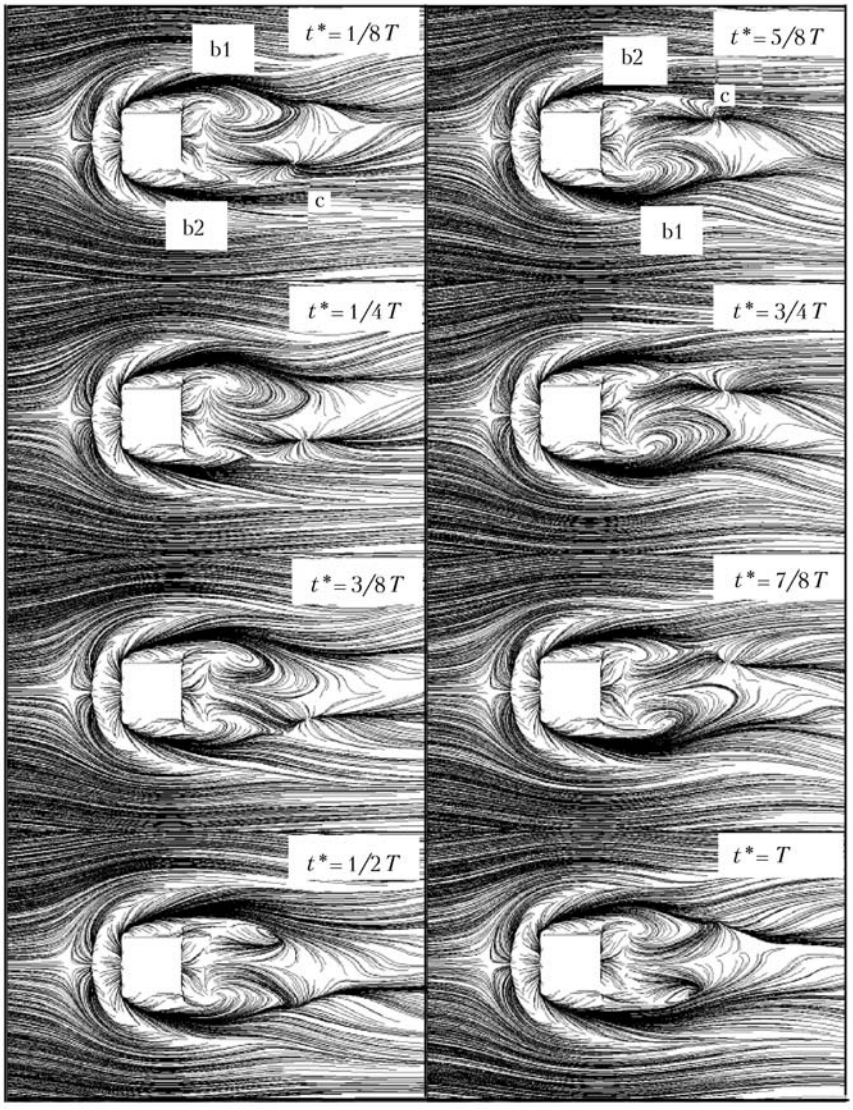

Fig. 6. Evolution of large-scale vortex flow structures, visualized using instantaneous patterns of spreading of the fluid on the lower channel wall, on one period of the self-oscillatory regime.

certain mismatch with the Martinuzzi experiment [1] where the characteristic Strouhal number St = 0.145 has been obtained. On the other hand, the results of direct numerical simulation of flow for a channel with a somewhat different geometry (h = 3) has shown St = 0.104 [17], which is close to the Strouhal number calculated in this work. The bimodal distribution of the horizontal and vertical velocity components is noted in both experiment [1] and direct numerical simulation [17].

CONCLUSIONS

1. We numerically investigate fully developed turbulent flow in the channel with a cube located on the wall for the Reynolds number Re = 40,000 on the basis of the FLUENT v6.3 package with unstructured tetrahedral and polyhedral grids. The methodology combining URANS (SIMPLEC method) and the modified SA turbulence model is tested.

2. A comparison of Martinuzzi's experimental data and the results of numerical predictions for the integral and local time-averaged characteristics of flow shows satisfactory agreement in the longitudinal distribution of the pressure coefficient on the lower wall of the channel and in the vertical profiles of the longitudinal velocity component in

the channel midsection. The vortex structure formed in separated flow past the cube and consisting of the horseshoe vortex, the attached forward, upper, and lateral vortices, and the arched and back detached vortices is identified. Computer visualization additionally shows the presence of the rear attached vortex behind the back wall of the cube.

3. An analysis of the self-oscillating regime of flow using fast Fourier transformation demonstrates the bimodal character of the process, which is due to the superposition of the oscillating motions of the arms of the horseshoe vortex and the rear arched and detached vortex structures (which is confirmed by experimental data [1]). The flow is characterized by two dominant Strouhal numbers: St = 0.09 and St = 0.175–0.185.

4. Satisfactory agreement, on the whole, between the calculated and experimental data for the test under study demonstrates the adequacy of application of the URANS computational methodology to the prediction of the characteristics of periodic turbulent separated flows.

This work was carried out with financial support from the Russian Foundation for Basic Research (project Nos. 08-08-90400, 08-08-90001, and 08-01-00059).

NOTATION

C_p, pressure coefficient; H, characteristic linear dimension, edge of the cube, m; h, height of the computational domain, in the fractions of H; L, length of the computational domain, in the fractions of H; Re and St, Reynolds and Strouhal numbers; T, period of oscillations; t^*, dimensionless time; W, width of the computational domain, in the fractions of H; U_x, U_y, and U_z, longitudinal, vertical, and transverse velocity components; U_b, mean-mass velocity; X, longitudinal dimension of the vortex in the fractions of H; x, y, z, horizontal, vertical, and transverse coordinates, in the fractions of H; y^+, dimensionless distance from the wall. Subscripts: f, position of the frontal saddle point of the attached horseshoe vortex; r1, dimension of the rear attached vortex; r2, dimension of the rear detached vortex; b, mean-mass, bulk.

REFERENCES

1. H. J. Hussein and M. Martinuzzi, Energy balance for turbulent flow around a surface mounted cube placed in a channel, *Phys. Fluids*, **8**, No. 3, 764–780 (1996).
2. http://cfd.me.umist.ac.uk/ercoftac/index.html.
3. G. Iaccarino, A. Ooi, P. A. Durbin, and M. Behnia, Reynolds- averaged simulation of unsteady separated flow, *J. Heat Fluid Flow*, **24**, 147–156 (2003).
4. W. Rodi, J. H. Ferziger, M. Breuer, and M. Pourquie, Status of large eddy simulation: results of a workshop, *J. Fluid Eng.*, **119**, 248–262 (1997).
5. K. B. Shah and J. H. Ferziger, A fluid mechanicians view of wind engineering: large eddy simulation of flow past a cubic obstacle, *J. Wind Eng. Industr. Aerodyn.*, **67**, 211–224 (1997).
6. P. A. Durbin, Separated flow computations with the k–ε–v^2 model, *AIAA J.*, **33**, No. 4, 659–664 (1995).
7. Fluent Inc. Fluent 6.3. Users Guide. Lebanon (2006).
8. S. A. Isaev, P. A. Baranov, N. A. Kudryavtsev, D. A. Lysenko, and A. E. Usachov, Comparative analysis of the calculation data on an unsteady flow around a circular cylinder obtained using the VP2/3 and FLUENT packages and the Spalart–Allmaras and Menter turbulence models, *Inzh.-Fiz. Zh.*, **78**, No. 6, 148–163 (2005).
9. S. A. Isaev, P. A. Baranov, N. A. Kudryavtsev, D. A. Lysenko, and A. E. Usachov, Complex analysis of algorithms, grid structures, and turbulence models in calculation of a circulation flow in a cavity using the VP2/3 and FLUENT packages. 1. Influence of schematic factors, *Teplofiz. Aéromekh.*, **12**, No. 4, 587–608 (2005).
10. S. A. Isaev, P. A. Baranov, N. A. Kudryavtsev, D. A. Lysenko, and A. E. Usachov, Complex analysis of algorithms, grid structures, and turbulence models in calculation of a circulation flow in a cavity using the VP2/3 and FLUENT packages. 1. Estimation of the adequacy of the models, *Teplofiz. Aéromekh.*, **13**, No. 1, 63–73 (2006).
11. P. Spalart and S. Allmaras, *A One-Equation Turbulence Model for Aerodynamic Flows*, Technical Report, AIAA-92-0439, American Institute of Aeronautics and Astronautics (1992).

12. B. R. Hutchinson and G. D. Raithby, A multigrid method based on the additive correction strategy, *Numer. Heat Transfer*, **9**, 511–537 (1986).
13. B. P. Leonard and S. Mokhtari, *ULTRA-SHARP Nonoscillatory Convection Schemes for High-Speed Steady Multidimensional Flow*, NASA TM 1-2568 (ICOMP-90-12), NASA Lewis Research Center (1990).
14. S. M. Rhee and U. L. Chou, Numerical calculation of a turbulent flow past a profile with separation at the trailing edge, *Aérokosm. Tekh.*, **2**, No. 7, 33–43 (1984).
15. J. P. Vandoormaal and G. D. Raithby, Enhancements of the SIMPLE method for predicting incompressible fluid flows, *Numer. Heat Transfer*, **7**, 147–163 (1984).
16. J. H. Ferziger and M. Peric, *Computational Methods for Fluid Dynamics*, Heidelberg, Berlin (1999).
17. A. Yakhot, H. Liu, and N. Nikitin, Turbulent flow around a wall-mounted cube: A direct numerical simulation, *J. Heat Fluid Flow*, **27**, No. 6, 994–1009 (2006).